A rock–ice avalanche without yield strength caused the 2026 Bhote Koshi–Trishuli flood, Nepal

Hyoseok Park[1,*]
[1]Department of Physics, Chungnam National University, Daejeon, Republic of Korea
*phs137@o.cnu.ac.kr

Preprint, not peer reviewed. Submitted to EarthArXiv, September 2026.

Abstract

On 26 August 2026 a rock–ice avalanche from the north face of Langtang Lirung, Nepal, produced a debris flow and flood that destroyed the Rasuwagadhi–Gyirong border crossing within eight minutes and reached Devghat, 180 km downstream, six hours later. We reconstruct the cascade with a depth-averaged mixture-flow model on the observed terrain, constrained by the seismic origin time, a CCTV frame, the gauge outages in the gorge, satellite-mapped trimlines and the stage records of four downstream gauges. The arrival times in the gorge are reproduced only if the moving mass had no yield strength (basal friction below 0.005), which we attribute to ice at the grain contacts; the energy of the fall then melted most of the ice within minutes. The gorge flow heights, the gauge records and the melting constraint jointly constrain the moving volume to 27 (18–35)$\times 10^6$ m^3, consistent with the mapped detachment, and the ice fraction to 0.1–0.3, whereas the seismic force alone requires a three- to fivefold larger source. Storage on the valley floor, about 25×10^6 m^3, controlled the flood wave below Syabrubesi. No glacial lake, landslide dam or stored water is required to explain the flood.

Introduction

Rock–ice avalanches that turn into long-runout floods are the most destructive process chain of the high mountains [1–4]. In the Himalaya they share their corridors with glacial-lake outburst floods, whose hazard and geomorphic work are far better documented [5–7], and the 2016 Bhote Koshi outburst flood ran down the same gorge as the 2026 event [6]. The 2021 Chamoli disaster showed how a seismically dated release, satellite mapping, eyewitness video and flow modelling together fix the sequence of such a cascade [1, 8]. Two questions remained open there. How does a granular mass of rock and ice acquire the mobility of a flood within minutes of the release, and what controls the flood wave once it leaves the mountains?

The 26 August 2026 Langtang event is the first cascade of this class with a hydrometric record over its full length in addition to the Chamoli-type constraints. A seismically dated release (02:52:10 UTC; M 5.2 USGS, M_w 5.7 GFZ), a CCTV frame 21 km downstream and eight stations of the Department of Hydrology and Meteorology bracket the front from the source to 180 km: Rasuwagadhi and Syabrubesi were destroyed in the gorge, Betrawati lost its telemetry, Malekhu was destroyed after crossing its warning level, Galchhi, Kali Khola and Devghat recorded the wave, and Dhunche, off the path, recorded nothing. Satellite mapping fixes the affected surface, the height reached on the gorge walls and the elevation change of the channel, the products that the 2015 Gorkha earthquake response established for this region [9].

We use these records to answer the two questions with a forward model scored against acceptance criteria defined from the records (Methods). The reconstruction is one process chain: the release lost its friction at the ice–rock contacts as it began to move, melted its ice in the fall, moved through the gorge as a solids-rich mixture with the solids and water travelling together, and entered the Trishuli as a surge whose downstream evolution was governed by the storage capacity of the valley floor. No source of water other than the release and the river is needed.

Results

The mass crossed the gorge with no yield strength

The apparent friction of the event, the drop divided by the distance travelled, is 0.125 to Rasuwagadhi and 0.086 to Syabrubesi, the same as the 0.11 of the Kolka–Karmadon rock–ice avalanche [10] and within the 0.05–0.11 that back-analyses give for this class [11]. The model reproduces this apparent friction through the impact and the turbulent resistance of the channel; its total dissipation to Syabrubesi is equivalent to a friction of 0.14. What the timing constrains is the Coulomb part of the resistance, the yield strength that decides whether a mass at rest on a 2% slope moves at all. Figure 1 shows the flow at 30 m resolution from the release to Syabrubesi, 36 km along the channel. The three timing constraints of the upper corridor are the CCTV frame at Gyirong Port (463(90) s after onset), the loss of telemetry at Rasuwagadhi (170–770 s) and at Syabrubesi (770–1370 s). With the roughness calibrated on the corridor ($n_w = 0.021$, Methods) the front reaches Gyirong Port at 420 s, Rasuwagadhi at 420 s and Syabrubesi at 1020 s on the 30 m grid (1140 s on the 60 m corridor grid). Over a grid of basal friction and roughness with everything else held (Fig. 2) the three windows are met together only with no friction, $\mu_s \leq 0.005$, and the roughness of a river, $n \leq 0.025$; a friction of 0.01 misses the Syabrubesi window at any roughness, and a roughness of 0.03 misses it even without friction. Narrowing the modelled gorge to its single-cell width moves the roughness bound to 0.03 and leaves the yield bound where it is. The super-elevation speeds mapped in the same reach, which do not depend on the telemetry, fall from 0.67 of the mapped value without yield strength to 0.48 with 0.02. Ice is the constituent that can remove the yield strength of a granular mass. In rotating-drum experiments the bulk friction of gravel–ice mixtures falls linearly with the ice content and mixtures above 40% ice liquefy [12]; two-phase rock–ice models reproduce the mobility of Kolka–Karmadon only with the friction reduced by the ice [13]. Gyirong Port and Rasuwagadhi, 21 and 22 km from the source, are insensitive to friction up to 0.02: the constraint comes from the 14 km of 2% gorge between Rasuwagadhi and Syabrubesi, where a mass with a Coulomb yield strength creeps at 1–3 m/s and a yield-free mixture runs at 10–20 m/s.

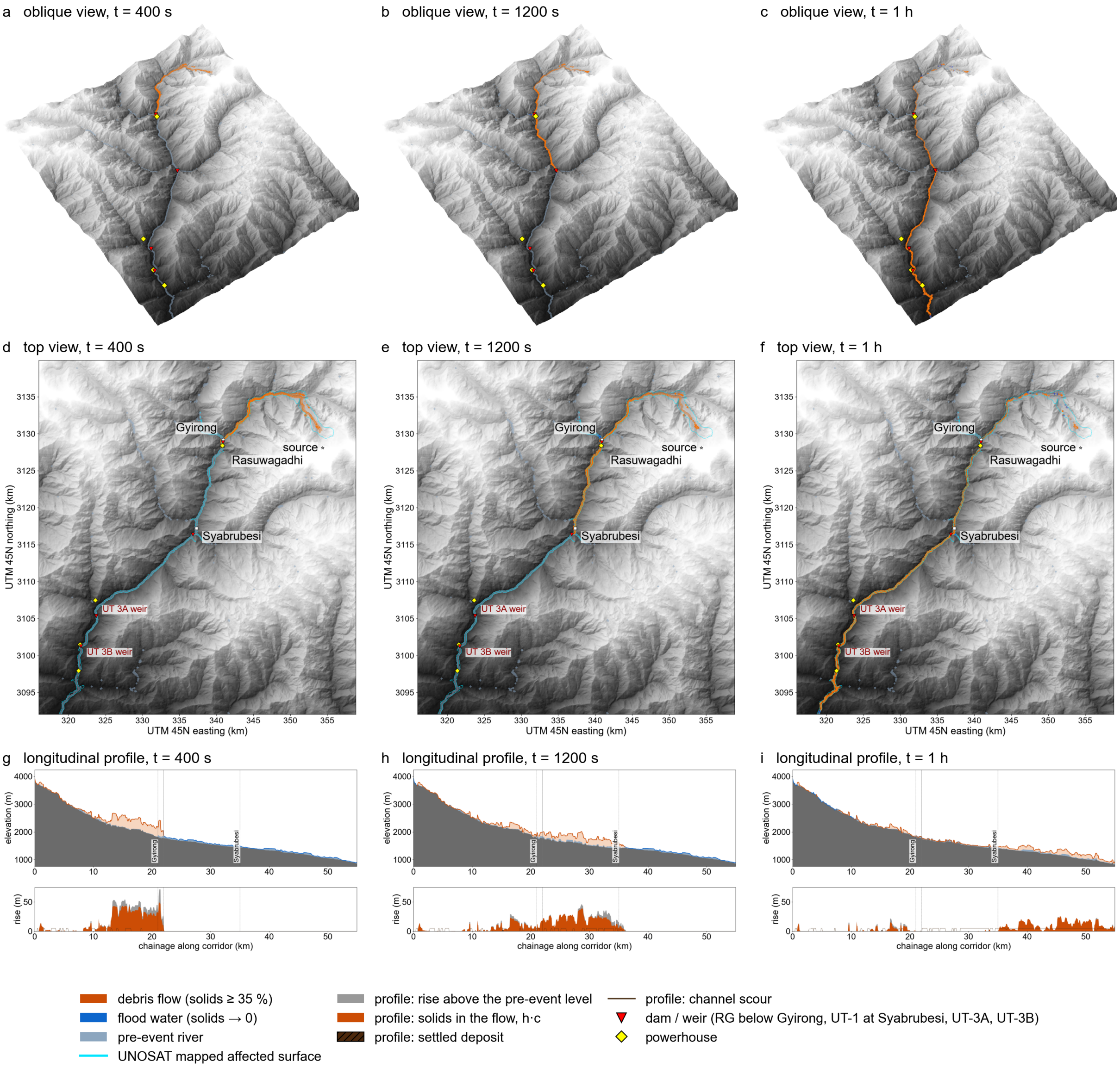

Figure 1: The release crossing the gorge. Oblique (a–c) and plan (d–f) views and the longitudinal profile (g–i) of the reconstruction on the 60 m corridor grid, 10 s output, at 400 s (the front at Gyirong Port and Rasuwagadhi), 1200 s (Syabrubesi) and 3600 s. Orange, mixture with more than 35% solids; blue, diluted flood water; cyan, the UNOSAT affected surface. The profile shows the bed, the flow (thickness exaggerated eight times) and, below, the rise of the surface above the pre-event river at true scale with the solids share of the flow, the settled deposit and the channel scour. Red triangles mark the Rasuwagadhi hydropower dam below Gyirong Port, the Upper Trishuli-1 dam at Syabrubesi and the Upper Trishuli 3A and 3B weirs; yellow diamonds the powerhouses.

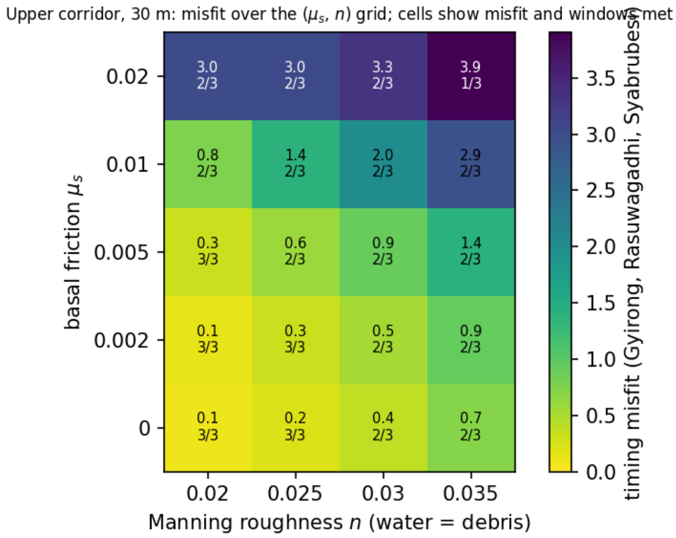

Figure 2: Timing misfit over basal friction and roughness. Mean squared deviation of the three upper-corridor arrivals from the centres of their windows, in units of the half-widths, over a grid of μ_s and n on the 30 m grid with all other parameters at their final values; each cell also gives the number of windows met. All three windows are met for $\mu_s \leq 0.005$ at $n = 0.02$ and for $\mu_s \leq 0.002$ at $n = 0.025$; at $n \geq 0.03$ the Syabrubesi window is missed at any friction, and $\mu_s \geq 0.01$ misses it at any roughness.

The constraint is on the material, not on the water supply, and it does not fix the volume: every release of the volume grid below meets the three windows without yield strength, and the seismic force inversion for this event (1.1–2 $\times 10^{12}$ N, EarthScope, quoted as 200–490 $\times 10^6$ m^3) and the satellite reconstruction calibrated on the Galchhi rise and the trimlines (100 $\times 10^6$ m^3, ±40% [14]) both point to a mass several times the mapped detachment.

The gorge and the gauges fix the moving mass

We therefore inverted the record for the release volume and the ice fraction together (Fig. 3), scoring every cell of a grid of six volumes (18–106 $\times 10^6$ m^3) and three ice fractions (0.1–0.3; 0.5 is excluded by the melting bound at the mapped volume, Supplementary Fig. S1) against four groups of evidence with the same misfit definition (Methods): the seismic force (peak and duration of the long-period inversion), the flow heights in the gorge (the trimline median of 59 m over the first 22 km and the 27 m rise at Rasuwagadhi and Syabrubesi), the fifteen timing, stage and volume criteria of Table 1 (three arrivals in the gorge, twelve at the five stations below Syabrubesi), and the requirement that the ice melts in transit. The evidence separates cleanly. The force on the Earth depends on the volume alone, at any ice fraction: 3.3×10^{11} N for the mapped 35×10^6 m^3 and 1.2×10^{12} N for three times that, so it reaches the seismic inversion only for about 100–160 $\times 10^6$ m^3. The gorge admits 18–35 $\times 10^6$ m^3: the trimline median is 55–69 m for these volumes, 82 m at 53×10^6 m^3 and 100 m or more above, and the gauge criteria, scored with the storage section fitted at the mapped volume, prefer the same range, with the lowest misfit at 27–35 $\times 10^6$ m^3 and a threefold rise at 106×10^6 m^3, where the Devghat excess volume of 33×10^6 m^3 exceeds the reported 10–30 $\times 10^6$ m^3 and the Galchhi rise doubles. This preference is partly degenerate with the storage: refitting the storage section for each volume lowers the gauge misfit of the 106×10^6 m^3 release from 4.9 to 2.8, against 2.4 for 27×10^6 m^3 (Methods), so the exclusion of large volumes rests on the flow heights in the gorge. The energy bound on melting does not resolve 0.1 from 0.2 and admits an ice fraction of 0.3 only where the fall releases enough energy: at that fraction 87% of the ice melts within two hours at 18×10^6 m^3 and 94–95% at 27–35 $\times 10^6$ m^3. Over the four groups together the best cell is 27×10^6 m^3 at 0.1–0.2 ice, and the cells within one misfit unit of it span 18–35 $\times 10^6$ m^3 and ice fractions of 0.1–0.3: the acceptable band contains the mapped detachment, 1.96 km^2 of scar at the 18 m mean thickness of the QHNU estimate, or 35×10^6 m^3, and the ice was between a tenth and a third of the release. The reference run of this paper uses the mapped volume, the one measurement of the release that is independent of the flow record, with an ice fraction of 0.2. The seismic force is the one record that this mass cannot satisfy: it requires three to five times the mapped volume, and we return to it below. The same heights bear on the resolution of the model: between Rasuwagadhi and Syabrubesi the reference run reaches 1.26 times the Planet trimline and 0.67 times the super-elevation velocity at 13 bends, so the modelled section is wider and slower than the real gorge, which the 30 m terrain cannot resolve and the low calibrated roughness compensates (Supplementary Note 4). The material did not stop in the gorge: the mapped elevation change between 20 and 46 km is 3.1×10^6 m^3 of erosion against 0.8×10^6 m^3 of deposition, and the reconstruction gives 5.5×10^6 m^3 and 2.0×10^6 m^3 in the same reach.

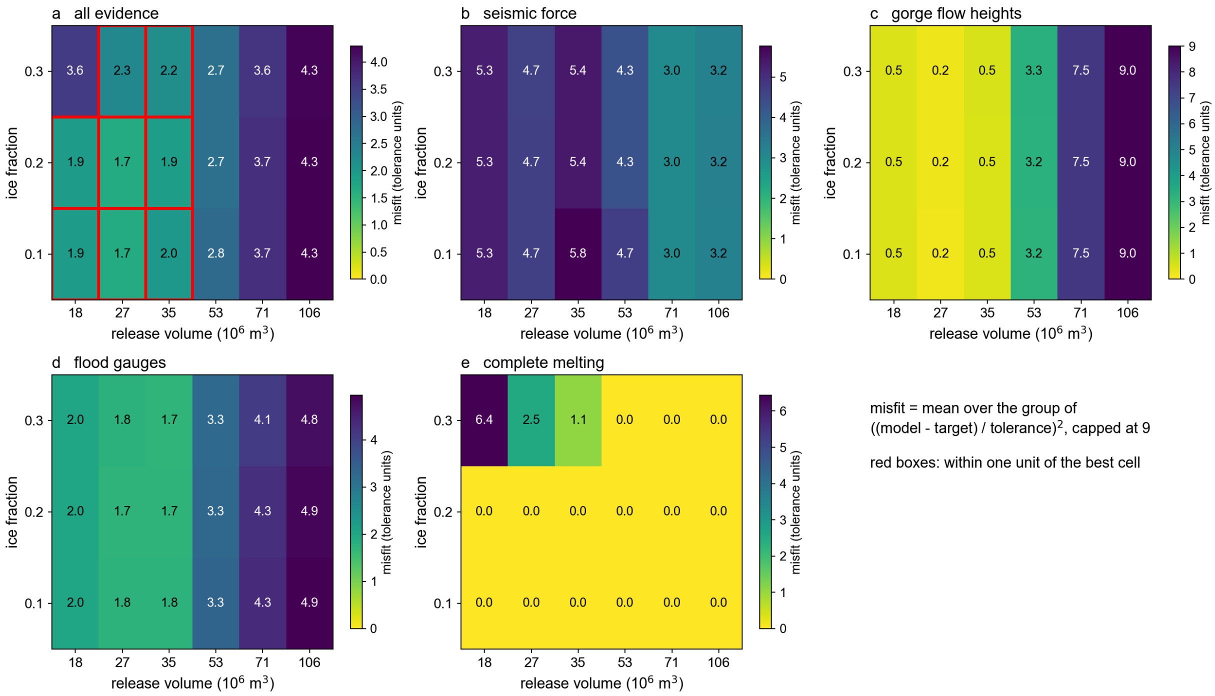

Figure 3: Inversion for the release volume and the ice fraction. Misfit, in units of the tolerance of each criterion, over a grid of six release volumes and three ice fractions, for all evidence together (a; red boxes, within one unit of the best cell) and for each group: the seismic force peak and duration (b), the flow heights in the gorge (c), the fifteen timing, stage and volume criteria of Table 1 (d) and the energy bound on complete melting within two hours (e). The gorge and the gauges admit 18–35 $\times 10^6$ m^3; the seismic force alone would need three to four times more.

Two further tests bound the process. A two-phase version of the model (Supplementary Note 1), in which solids and water have separate velocities coupled by drag, meets the same windows (360, 360 and 900 s against 420, 420 and 1020 s) with the same composition whether the drag locks the phases or lets the fluid run ahead of the solid (Supplementary Note 1, Supplementary Table S1): a leading 2 km with a depth-weighted solids fraction of 0.3–0.5 and a body of 0.7–0.78 behind it, the same structure that the single-fluid run shows (0.2–0.5 and 0.70–0.74); the two-phase runs are 60–120 s faster than the single-fluid run because only their fluid fraction feels turbulent resistance, and that is the physics behind the calibrated $n_d < n_w$. Separation of water from solids therefore played no part in the gorge, and the front was a solids-rich mixture rather than a water wave running ahead of a debris body. The force that the moving mass exerted on the Earth, $-\mathrm{d}\mathbf{P}/\mathrm{d}t$ with $\mathbf{P}$ its momentum (Supplementary Fig. S2), peaks at 3.3×10^{11} N at 35 s for the mapped volume released with the free-fall speed of the 1.1 km drop from the mean source elevation to the valley floor, when the mass reaches that floor, reverses within 20 s and rings with a 50–60 s period as the flow turns down the valley; released at rest the peak is 6% lower, so the peak is set by the impact and not by the way the detachment is prescribed. The peak depends on the released volume alone (Fig. 3b) and reaches the long-period inversion for the event (1.1–2×10^{12} N over 88 s, EarthScope rapid product [15], by the method of Ekström and Stark [16]; see also Allstadt [17]) only for about 100–$160 \times 10^6\,\mathrm{m}^3$; the modelled force also rings to 300 s where the inversion ends at 88 s, because the later oscillations are those of the flow in the valley and not of the source. The seismic record therefore points to a more violent release than the mass that reached the river as a flow. The radiated energy of the recorded event, 4×10^{12} J for M 5.2 or 2×10^{13} J for M_w 5.7, is 0.1–0.7% of the 2.9×10^{15} J of potential energy released to Syabrubesi, within the 10^{-4}–10^{-2} seismic efficiency of large rock avalanches [16].

Ice at the grain contacts removed the friction; the fall melted the rest

The release is rock and ice with no free water. The river between the source and Syabrubesi held $2.1 \times 10^6\,\mathrm{m}^3$, and one hour of inflow adds $0.9 \times 10^6\,\mathrm{m}^3$, against a release of $35 \times 10^6\,\mathrm{m}^3$; the water that liquefied the mass had to be made on the way. The mechanical energy that the mass loses, in the impact on the valley floor, in the collisions of rock with rock and rock with ice, and at the bed, is 3.8×10^{15} J over the corridor in eight hours, a total that includes the descent of the river water and of the entrained channel fill, against a potential-energy release of 2.9×10^{15} J to Syabrubesi and 3.8×10^{15} J to Galchhi for the 9.4×10^{10} kg that the model assigns to the release (the solids density of $2650\,\mathrm{kg/m}^3$ for rock and ice alike, Methods; mean source elevation 4530 m), and in the reconstruction all of it goes into the mixture as heat. With a fifth of the release as ice ($7.1 \times 10^6\,\mathrm{m}^3$) the energy available melts 65% of the ice in three minutes (Fig. 4), 87% by Gyirong Port, 97% within two hours and all of it within the day (Supplementary Fig. S3). This is the energy bound on the melting, not its kinetics: the model melts ice wherever heat is released, which requires the ice to be broken to centimetre scale in the fall, as the Kolka–Karmadon deposits showed [18]; metre-scale blocks would melt over hours. The bound is what matters for the composition. A release with more ice reaches the Trishuli with ice in it: within two hours 95% of the ice has melted at an ice fraction of 0.3 in the inversion runs, and in the sweep released at rest, which dissipates less energy early, 83% at 0.3, 65% at 0.4 and 53% at 0.5 (Supplementary Fig. S1). No ice has been reported in the flood or its deposits below the gorge, and the published descriptions of the event treat the ice as melted in transit [14, 19]; if that is confirmed by the field survey, the ice fraction was at most 0.3.

The meltwater did not, however, liquefy the mass in the sense of a saturated granular body. Even at 0.2 the mixture below Rasuwagadhi is a quarter water by volume, less than the 0.36 that fills the pores of a packed granular mass, and at the impact at 40 s only 4% of the volume is meltwater. When the friction is made to depend on the local water content, so that a dry mass is frictional until its pores fill with meltwater, the timing fails in every variant tried (Supplementary Note 2): the front reaches Gyirong Port at 540–1680 s and Syabrubesi at 2100 s or never, and doubling the ice to 0.4 does not help, because a slower mass dissipates less energy early and melts less. The mobility was therefore acquired before the bulk meltwater existed, in the first seconds of motion. Ice at the grain contacts, where a film of melt costs a negligible fraction of the energy budget, is the mechanism consistent with this constraint; it is the mechanism inferred for Kolka–Karmadon and Chamoli [1, 18], and it is what the yield-free single-fluid model and the two-phase model with a pore-pressure ratio of one both represent. It requires ice at the contacts throughout the mass, and therefore an ice fraction that is not small; the record does not fix a lower bound, and hanging-glacier detachments of this class carry 0.1–0.3 of ice by volume [1]. The gauge records cannot sharpen the ice fraction either: melting changes the composition of the mixture and not its volume, and the routed surge at the four lower gauges is the same for any ice fraction from 0.1 to 0.8 (Supplementary Fig. S1); what the ice fraction changes is the solids that settle along the Trishuli, which the post-event survey can measure. Dilution by the river follows down the gorge: the flux-weighted solids fraction of the mixture passing Rasuwagadhi is 0.75, at Syabrubesi 0.56 at the front and 0.71 over the event, and at Betrawati 0.39 at the front; the mass reaches the Trishuli as a hyperconcentrated flow with most of its solids still in it.

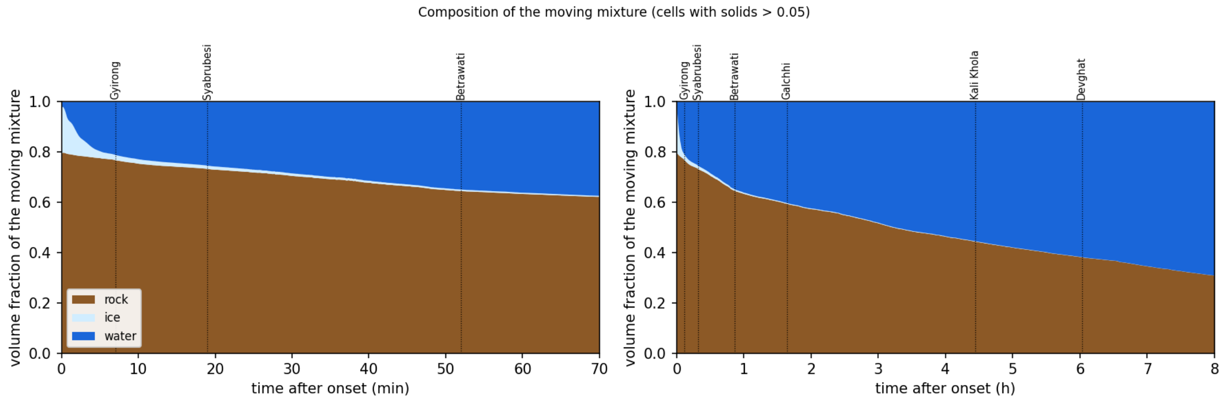

Figure 4: Composition of the moving mixture. Volume fractions of rock, ice and water in the cells with more than 5% solids, over the first 70 min (left, output every 10 s) and over eight hours (right): the release is rock and ice, the ice melts within minutes, and the river dilutes the mixture down the corridor. Heat from the fall, the river, the cooling rock and the air are all included (Methods).

Valley-floor storage set the flood wave below Syabrubesi

The four gauges below the gorge record the rise at Galchhi (80 km) at 1.6–2.2 h after onset with a peak of 8.8 m at 1.9–2.6 h, the Malekhu warning level (105 km) at 2.65–2.8 h before the station was destroyed, the rise at Kali Khola (148 km) at 4.5–5.2 h with 5.6 m, and at Devghat (180 km) at 5.9–6.05 h with a 1.9 m rise, a peak 1.7–2.8 times the base flow at 7.4 h and an excess volume of 10–30 × 10^6 m^3; the Betrawati station (46 km) stopped reporting at 2570–3170 s. The mixture leaving the gorge, above the base flow, is 38 × 10^6 m^3 passing Rasuwagadhi at a peak of 1.1 × 10^5 m^3/s lasting ten minutes and 50 × 10^6 m^3 passing Syabrubesi after entrainment and dilution at a peak of 2.7 × 10^4 m^3/s. Routed down a channel of the mapped width on the mapped profile (Methods), this surge is too fast and too sharp: Galchhi at 1.2 h, Devghat at 4.4 h, a peak four times the base flow. Routed on the 60 m grid, on which the surge spreads over the valley floor, it is too slow: Galchhi at 2.2 h and Devghat after 8 h, and a 24-run sweep of the six corridor parameters cannot change this (Supplementary Fig. S5). The observed wave lies between the two and the difference is storage.

We therefore route the surge through a compound section: the mapped channel conveys the flow and the valley floor above the bank stores water without conveying it. Its two parameters, the bank height above the pre-event river and the storage width, were fitted on the Galchhi and Devghat records alone over a 50-run grid (Supplementary Fig. S6). The misfit is low along a band on which the product of the two, the storage capacity per unit length, is nearly constant, with its best cell at a bank height of 3 m and a storage width of two channel widths; the data identify the storage volume, not the two parameters separately, the cells within one misfit unit of the best span a storage capacity of 2–9 m times the channel width, and the radar terrain gives independently a valley floor within 4 m of the river of 0.5–1.0 channel widths along the Trishuli (median 0.76, interquartile range 0.52–1.02; Methods), a capacity of about 3 m times the channel width, inside that band. The three held-out gauges are then predictions of the best-fit routing: Betrawati at 3120 s (window 2570–3170 s), the Malekhu warning level at 9420 s (9540–10140 s) and the Kali Khola rise at 4.43 h (4.5–5.2 h). Figure 6 shows the wave over the full corridor at 1, 3 and 6 h; Fig. 5 and Table 1 give the ensemble of the three routings within one misfit unit of the best on the eight Galchhi and Devghat criteria: the Galchhi rise at 1.63–1.82 h and peak at 2.0–2.4 h, the Malekhu warning level at 8940–9900 s, the Kali Khola rise at 4.35–4.65 h, the Devghat rise at 6.0–6.3 h and peak at 7.0–7.4 h with a rise of 2.1–2.5 m, a peak 2.6–3.0 times the base flow and an excess of 16–22 × 10^6 m^3. The Galchhi arrival and peak fall inside their windows, Malekhu and Kali Khola are 4–10 min early and the Devghat rise 0–15 min late, while the stage rises at Galchhi (3.9–5.6 m against 8.8 m) and Kali Khola (2.8–3.1 m against 5.6 m) are low by a third to a half although the timing and the Devghat rise are met; no 2026 rating exists at Galchhi or Kali Khola, so whether the residual lies in the wave or in the cross-sections at the gauges is open. The storage that the routing requires, 23–28 $\times 10^6\,\mathrm{m}^3$ over 130 km of valley floor, is the difference between the excess volume that the routed surge carries past Galchhi (44–45 $\times 10^6\,\mathrm{m}^3$) and past Devghat (16–22 $\times 10^6\,\mathrm{m}^3$); the routing has no settling, so the $19 \times 10^6\,\mathrm{m}^3$ of solids that the corridor model deposits below Betrawati is a separate, corridor-model quantity (Supplementary Note 3). The water of the flood is the release, its meltwater and the river: the seven-day DHM record before the event shows no impoundment on the Bhote Koshi, the stage at Rasuwagadhi falling smoothly from 2.05 to 1.75 m and at Syabrubesi from 4.33 to 3.93 m over the last 72 h, the late-monsoon recession, with no step that a dam holding the river ($150\,\mathrm{m}^3/\mathrm{s}$, $13 \times 10^6\,\mathrm{m}^3$ per day) would have produced.

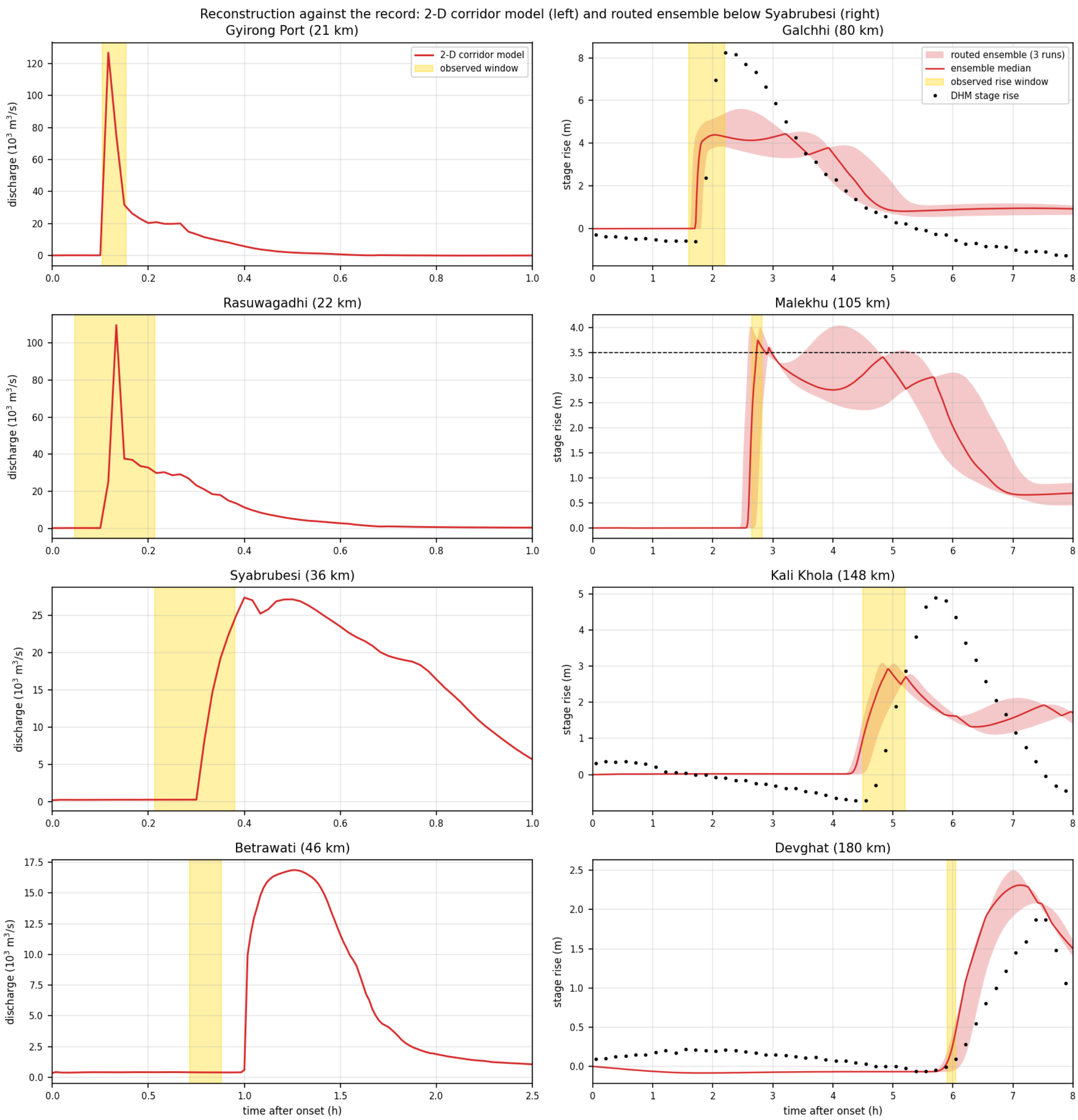

Figure 5: Reconstruction against the record. Left, discharge through the transects at the four upper sites from the corridor model with the observed windows. Right, stage rise at the four lower gauges from the routed ensemble (band, three members; line, median) with the DHM records (stage minus the pre-onset level) and the observed rise windows; at Malekhu the dashed line is the last reading above the warning level.

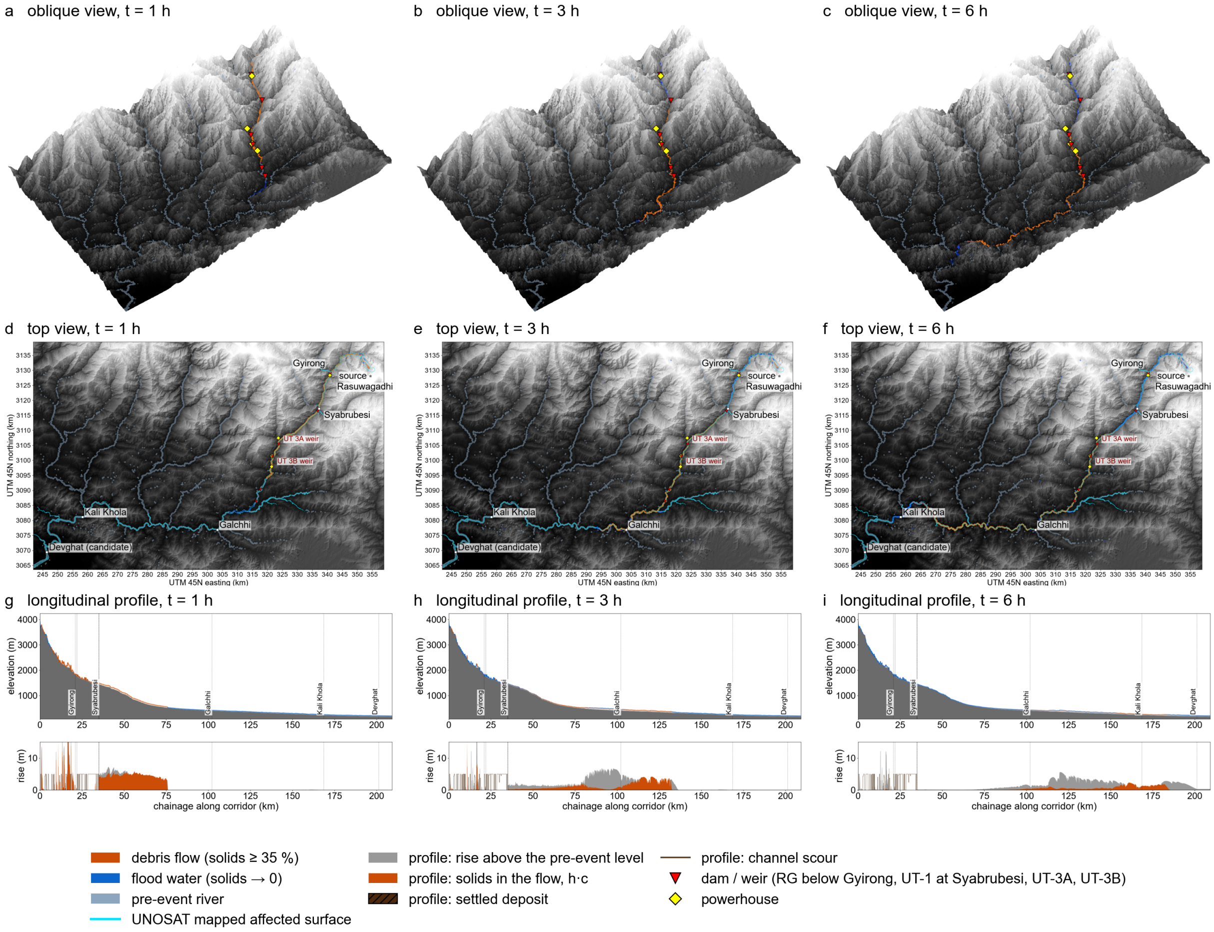

Figure 6: The flood wave over the full corridor. Oblique (a–c) and plan (d–f) views and the longitudinal profile (g–i) of the reconstruction from the source to Devghat at 1, 3 and 6 h after the release, 60 s output, with the same colours and symbols as Fig. 1. Below Syabrubesi the profile shows the one-dimensional routing with the compound section (channel and valley-floor storage) that provides the downstream results, at true scale in the lower panel of each profile; the plan views show the corridor model on its 60 m channel. The hydropower dams and weirs of the corridor are marked as in Fig. 1.

Table 1: Acceptance criteria (time after 02:52:10 UTC) and the reconstruction. Upper sites: 30 m corridor model, output every 60 s. Lower sites: range over the routed ensemble. Tolerances are the half-widths used in the misfit; ✓ within the window, ∼ within one tolerance of it, × outside.

Site (chainage)	Observation	Criterion	Reconstruction	
Gyirong Port (21 km)	CCTV frame	arrival 373–553 s	420 s	✓
Rasuwagadhi (22 km)	telemetry lost	170–770 s	420 s	✓
Syabrubesi (36 km)	telemetry lost	770–1370 s	1020 s	✓
Rasuwagadhi–Syabrubesi	Planet trimline	height ratio 1	1.26	∼
Rasuwagadhi–Syabrubesi	super-elevation	speed ratio 1	0.67	×
Betrawati (46 km)	telemetry lost	2570–3170 s	3000–3240 s (best fit 3120)	∼
Galchhi (80 km)	DHM stage	rise 1.6–2.2 h	1.63–1.82 h	✓
		peak 1.9–2.6 h	2.0–2.4 h	✓
		rise 8.8 m ± 1	3.9–5.6 m	×
Malekhu (105 km)	warning level	9540–10140 s	8940–9900 s (best fit 9420)	∼
Kali Khola (148 km)	DHM stage	rise 4.5–5.2 h	4.35–4.65 h (best fit 4.43)	∼
		rise 5.6 m ± 0.7	2.8–3.1 m	×
Devghat (180 km)	DHM stage	rise 5.9–6.05 h	6.0–6.3 h	∼
		peak 7.4 ± 0.25 h	7.0–7.4 h	✓
		rise 1.9 m ± 0.4	2.1–2.5 m	∼
Devghat	situation report	peak ratio 1.7–2.8	2.6–3.0	∼
		excess 10–30 × 10^6 m^3	16–22 × 10^6 m^3	✓
Dhunche (off path)	DHM stage	no rise	no rise	✓

Discussion

The 2026 flood is explained by the rock–ice collapse alone. A release of 35×10^6 m^3 of rock and ice, with no stored water, no lake and no dam, gives the eight-minute arrival at the border, the gorge trimline and channel erosion within a factor of 2 and channel deposition within 2.5, and the timing of the flood at four gauges to 180 km with the stage and volume at Devghat; inverted for the volume, the gorge and the gauges return 27 (18–35)$\times 10^6$ m^3, a band that contains the mapped detachment, with an ice fraction of 0.1–0.3. The mobility was not acquired in the gorge from the river, nor from the bulk meltwater, which did not yet exist when the mass was already moving without friction: the yield strength was gone from the first seconds, which is consistent with ice at the grain contacts, the energy of the fall then melted the bulk of the ice within minutes, and the state persisted through the gorge while the apparent friction of the run, 0.09–0.12, was set by the impact and the channel; in the two-phase model this is the state of a pore-pressure ratio near one, in the single-fluid model a basal friction below 0.005, and both are the same physics. The volume that reached Devghat is the release and its meltwater delivered through a storing valley, and the gauge record of the week before the event shows no impoundment on the Bhote Koshi: no other source of water is required. The volume budget alone cannot exclude a small one, because an extra 5×10^6 m^3 of lake water is degenerate with a 20% change in the fitted storage; a tributary of the release valley impounded for a day would hold 1×10^6–3×10^6 m^3, a tenth of the release, and would not change the reconstruction. The one alternative that the timing admits, a release several times larger than the mapped detachment moving with ordinary friction, is excluded by the flow heights on the gorge walls and by the volume that reached Devghat (Fig. 3), but it is the alternative that the seismic force inversion favours, and the 100×10^6 m^3 of the satellite reconstruction [14], calibrated on the Galchhi rise, is at the lower edge of what the seismic force requires and three times too large for the gorge and the gauges. The mass that the seismograms recorded and the mass that reached the river as a flow are therefore different quantities. The discrepancy would be reconciled if 65–125 $\times 10^6$ m^3 took part in the seismic source but did not enter the downstream flow, for example by remaining in the source basin or on the lower slope; the 2 m elevation-change products available to us cover the channel reaches only, and a post-event DEM of the source area would settle this. What happened in the first 90 s of the event, between the detachment that the seismograms recorded and the mass that crossed the border, is the open question that this reconstruction leaves.

Below the mountains the control changes from the material to the valley. The surge that left the gorge would have reached Devghat in four and a half hours had the Trishuli behaved as a channel of its mapped width; it took six because the valley floor stored 23–28 $\times 10^6\,\mathrm{m}^3$ on the way. Storage is a measurable property of the corridor and, unlike the rheology of the release, it can be surveyed in advance. For a release of this size in this season the record gives 1.6 h to Galchhi and 6 h to Devghat, and the routing shows why.

The public accounts of the event describe a four-stage chain in which the avalanche briefly dammed the Lhende Khola before the dam broke [14]; the blockage is estimated to have failed within a couple of minutes, and a pond of 0.5–1.5 $\times 10^6\,\mathrm{m}^3$ was left 2.4 km below the source. A blockage of that duration is shorter than the Rasuwagadhi window and is not resolved by the model, which does not need it. A pre-existing landslide dam, filled before the event, has also been proposed as the source of the flood water; the gauge record before the event shows no impoundment (Results), the flood volume at Devghat needs no stored lake, and the front in the gorge was a solids-rich mixture, not a water wave. A small pond in the tributary valley of the release cannot be excluded by the gauges, but the catchment above the source cannot supply a volume that matters.

Three residuals identify the measurements that would close them. The modelled flow height in the gorge is a quarter above the trimline and the depth-averaged speed a third below the super-elevation value, which together indicate a cross-section narrower than the 30 m radar terrain resolves. The stage rises at Galchhi and Kali Khola are low by a third to a half although the arrivals are met; without a 2026 rating at either gauge the residual cannot be assigned to the wave or to the cross-section. And the reconstruction predicts about 20 $\times 10^6\,\mathrm{m}^3$ of fresh sediment, 1–2 m thick, on the Trishuli valley floor between Betrawati and Galchhi (Supplementary Note 3), which post-monsoon imagery can test and which scales with the rock fraction of the release.

Methods

Terrain

The computational bed is the Copernicus GLO-30 radar DSM [20] (EPSG:32645, EGM2008) at 60 m over a 117×76 km window from the source to Devghat and at 30 m over a 26×28 km window from the source to Syabrubesi. Radar terrain in gorges contains closed depressions that block or store flow. A priority-flood pass defines D8 receivers [21]; depressions deeper than 15 m are filled, every channel path (contributing area $\geq 2\,\mathrm{km}^2$) is breached so that it descends by at least 5×10^{-4} per cell with four-connected diagonal steps, and the main stem is widened to two cells. Below Syabrubesi, where the radar DSM does not resolve the channel, the bed is a hydraulic-geometry channel: the longitudinal profile is the isotonic-regressed thalweg, joined to the conditioned bed at Syabrubesi, and the width follows the contributing area, anchored on pre-event water widths mapped from Sentinel-2 [22] (60 m in the gorge, 115 m at Galchhi, 200 m at $6000\,\mathrm{km}^2$, 400 m at Devghat). The valley-floor width used to check the routing is the area of DSM cells within 1.5 km of the channel and within 2, 4 or 8 m of the modelled pre-event water surface, per 2 km of route. The breached radar bed keeps a staircase of pools and steps along the main stem; filling every pool up to a ramp of half the local reach slope (28 m at most, 24 $\times 10^6\,\mathrm{m}^3$ of pool volume over the corridor) leaves the three gorge arrivals unchanged, moves the corridor-model arrivals below Syabrubesi by 4 min and changes entrainment and deposition by 1–5%, so the inversion grids use the breached bed and the animations the filled one.

Flow model

We solve the depth-averaged shallow-water equations for depth h, unit discharge (hu, hv), a solids tracer hc (c, solids volume fraction), an ice tracer hi and the sensible heat of the liquid hq with a

Godunov/HLL finite-volume scheme on the corridor cells only (3.1×10^5 cells at 60 m, 1.3×10^5 cells at 30 m). Bed slope is treated by hydrostatic reconstruction [23] with a depth-limited in-cell bed tilt; a lake at rest on a rough bed is preserved to 10^{-6} m/s and mass to 10^{-7}. The mixture is a fluid whose resistance follows the solids concentration [24–26]: $\tau/\rho_m h = g\mu_s c + g\,n(c)^2|\mathbf{u}|^2 h^{-4/3}$ with $\rho_m = 1000(1 + 1.65c)$ kg/m^3 and $n(c) = n_w + (n_d - n_w)c$; the solids tracer c counts rock and ice together at the solids density, so the dry release has $c = 1$ and $2650\,\text{kg/m}^3$, 15% above the $2300\,\text{kg/m}^3$ of a mixture with 20% ice; the ice tracer hi carries the ice share, and melting moves volume from hi to the liquid at constant h, which lowers c and the mixture density by 1650 kg per cubic metre melted. This bookkeeping overstates the mass of the release by up to 15% before melting and lets 12% of it disappear as the ice melts; the impact force peaks before most of the melting, so the force histories are high by at most 15%, a bias that works against the conclusion that the modelled force is too small. The corridor runs use $\mu_s = 0$, $n_w = 0.021$ and $n_d = 0.015$ from the sweep described below, and the release is rock and ice; $n_d < n_w$ expresses the damping of turbulence in a solid-laden column that the two-phase model produces without a parameter, and the low n_w absorbs the excess width of the 60 m channel. Melting consumes the heat store hq, which receives, at every step, the whole loss of mechanical energy of the flow (kinetic plus potential, evaluated before and after the flux and friction updates, less the energy leaving through the domain boundary), distributed over the wet cells in proportion to their momentum; the sensible heat of the river water at 12 °C; the sensible heat of the released rock cooling from 3 °C to the melting point (2.1×10^6 J/m^3/K, 1.8×10^{14} J); and a heat flux of 300 W/m^2 from the air and the sun to the wet surface. Ice melts at 3.0×10^8 J/m^3. The mechanical term dominates the first hour; the rock and air terms melt the ice that the flow strands in thin deposits. Crediting only the bed-friction work, as debris-flow models usually do, melts a tenth as much in the gorge (Supplementary Fig. S3), because a yield-free flow dissipates little at the bed and most of the loss occurs in the impact and in internal shear. Entrainment removes channel fill at $K(|\mathbf{u}| - u_c)_+$ where $c > 0.05$ ($K = 0.0074$, $u_c = 6$ m/s, 5 m available); solids settle where the flow is slower than $u_{\text{dep}} = 1.8$ m/s on a timescale $\tau_{\text{dep}} = 340$ s, raising the bed. The river is spun up for 48 h with a uniform runoff of 13.5 mm/day and boundary inflows on the Bhote Koshi (150 m^3/s), Budhi Gandaki (500 m^3/s) and Marsyangdi (700 m^3/s); the release is the UNOSAT detachment zone filled to 35.4×10^6 m^3 (mean thickness 18 m) of rock and ice with no free water, a fifth of the volume as ice in the reference run (the ice fraction is a free parameter of the inversion), released over 30 s with the free-fall speed (150 m/s) of the 1.1 km drop from the mean source elevation (4530 m) to the valley floor at the foot of the scar (about 3400 m), along the local downslope direction. Runs are executed in PyTorch on one GPU; an 8-hour corridor run takes 7 min, an hour on the 30 m grid 3 min.

Criteria, their changes, and the corridor sweep

Discharge and stage are extracted through 1.8 km four-connected transects normal to the route; arrival is the first 0.5 m rise above the pre-event stage or a doubling of the discharge, at the 60 s output cadence, so every arrival carries ±30 s. The Devghat transect crosses the Narayani at 84.428°E, 27.725°N, below the Kali Gandaki junction, with a base flow of 2750 m^3/s, consistent with the 2600 m^3/s of the situation report. At Gyirong Port the transect stage is taken over a side channel and does not rise, so the arrival there is the discharge criterion. The criteria of Table 1 were defined from the records before the model was run; the Galchhi and Kali Khola stage criteria were added when the DHM records became available, and the Malekhu warning-level crossing is scored with the window of the station's 10 min record (9540–10140 s). Stage rises are measured from the pre-onset level of each record (Galchhi 360.6 m to a peak of 369.45 m, Kali Khola 6.8 m to 12.35 m on the station datum). Over the seven-day record before the event the Rasuwagadhi telemetry dropped one packet in 1296 and the Syabrubesi telemetry 21, so the chance that a random dropout falls in a given ten-minute window is 0.1% at Rasuwagadhi and 1.8% at Syabrubesi; the two losses within the ten minutes in which the modelled front passes each station are taken as the front, and the super-elevation speeds mapped in the same reach constrain the same quantity independently (Results). Six corridor parameters were sampled in a 24-run

Latin hypercube at the mapped volume (n_w 0.020–0.035, n_d 0.012–0.029, initial solids fraction of the release 0.71–0.99, u_{dep} 1.6–6.0 m/s, τ_{dep} 160–2400 s, K 0.002–0.0095); the best run set the roughness, settling and entrainment values, and its initial water content (24%) was then replaced by rock and ice with energy-conserving melting, which leaves the arrivals unchanged. The ice fraction was then varied from 0.1 to 0.8 without friction, with each corridor run routed to Devghat with the fitted storage section (Supplementary Fig. S1). The Latin hypercube was scored by the mean over the 15 timing, stage and volume criteria of Table 1 (the trimline, super-elevation and off-path checks are not scored) of the squared deviation in units of the tolerance (Supplementary Fig. S5); the best run supplies the corridor reconstruction and the surge routed downstream.

Routing below Syabrubesi

The surge delivered at Syabrubesi by the corridor model (discharge and solids flux) is routed to Devghat with a one-dimensional Saint-Venant model on the same profile and mapped widths (HLL, hydrostatic reconstruction, Manning $n(c)$), with the lateral baseflow and the two boundary inflows at their junctions and an eight-hour pre-event spin. The compound section stores water above a bank height h_b above the pre-event river at a width W_s without conveying it; n_w takes 0.03 or 0.04 for the river reach, the routing has no settling, and the pre-event spin is 8 h so that the base stage is stationary to 0.1 m. $h_b \in \{1, 2, 3, 4, 6\}$ m and $W_s \in \{0.5, 1, 1.5, 2, 3\}$ channel widths were scored on the eight Galchhi and Devghat criteria only (Supplementary Fig. S6); the ensemble of Fig. 5 is the three routings within one misfit unit of the best on the same eight criteria, so Betrawati, Malekhu and Kali Khola enter neither selection; a peak that falls on the last output of a run is not counted as a peak.

Joint inversion for the release volume and the ice fraction

Six release volumes (0.5, 0.75, 1, 1.5, 2 and 3 times the mapped $35.4 \times 10^6\,\text{m}^3$, the detachment zone filled to the corresponding thickness) and three ice fractions (0.1, 0.2, 0.3) were run with the production parameters, each as a 900 s run on the 30 m grid stored every 5 s for the force history and the gorge heights and as an 8 h run on the 60 m corridor grid routed to Devghat with the fitted storage section ($n_w = 0.03$, bank 3 m, storage width two channel widths). The seismic tolerances are the half-width of the published force range (1.1–$2 \times 10^{12}\,\text{N}$) and a quarter of the published duration. Each cell is scored against four groups: the seismic force, with the peak of $|\text{d}\mathbf{P}/\text{d}t|$ against $1.55(45) \times 10^{12}\,\text{N}$ and the duration above 30% of the peak against 88(25) s; the gorge heights, with the median over 1 km bins of the maximum flow height on the thalweg over the first 22 km against the trimline median of 59(11) m and the stage rises at Rasuwagadhi and Syabrubesi against 27(8) m; the fifteen timing, stage and volume criteria of Table 1; and complete melting, scored as zero when 95% of the ice has melted within two hours and as the squared shortfall in units of 5% otherwise. The misfit of a group is the mean of the squared deviations in units of the tolerance, capped at 9, and the total misfit is the mean over the four groups; the acceptable region is the set of cells within one unit of the best. Because the storage section was fitted at the mapped volume, three cells (27, 53 and $106 \times 10^6\,\text{m}^3$ at 0.2 ice) were re-routed over a 3×3 grid of bank height (2–4 m) and storage width (1–3 channel widths): the best gauge misfit over the twelve criteria below Syabrubesi is 2.4, 3.2 and 2.8, against 2.4, 3.3 and 4.9 with the fixed section, so the gauges alone do not exclude the largest volume once the storage is free, and the flow heights in the gorge do.

Force history

The force on the Earth is $-\text{d}\mathbf{P}/\text{d}t$ with $\mathbf{P} = \sum \rho_m h \mathbf{u}\,\Delta x^2$ over the moving mass, from a 30 m run stored every 5 s; the vertical component uses the velocity along the bed. The seismic energy uses $\log_{10} E_s = 1.5M + 4.8$.

Data availability

Observations are from the UNOSAT product 4260 [27], the Planet and Geo-PERA disturbance and elevation-change products, the DHM stage records and the rapid-assessment reports [28–31]. The solver, the routing and inversion scripts, the figure and animation code, the parameter sets of every sweep and the observation registry are at `https://github.com/hyoseokp/langtang-2026-cascade` (MIT licence) and archived on Zenodo (`https://doi.org/10.5281/zenodo.22549896`); the corridor grids, the stored run outputs used for every figure and the rendered animations are in the same Zenodo record. The five animations (gorge: oblique, plan and longitudinal-profile views at 10 s; full corridor: plan and longitudinal-profile views at 60 s), the corridor grids and the production run outputs are in the Zenodo dataset record `https://doi.org/10.5281/zenodo.22549201`.

References

[1] D. H. Shugar, M. Jacquemart, D. Shean, et al. A massive rock and ice avalanche caused the 2021 disaster at Chamoli, Indian Himalaya. *Science*, 373(6552):300–306, 2021. doi: 10.1126/science.abh4455.

[2] A. Kääb, M. Jacquemart, A. Gilbert, et al. Sudden large-volume detachments of low-angle mountain glaciers – more frequent than thought? *The Cryosphere*, 15:1751–1785, 2021. doi: 10.5194/tc-15-1751-2021.

[3] Andreas Kääb, Silvan Leinss, Adrien Gilbert, Yves Bühler, Simon Gascoin, Stephen G. Evans, Perry Bartelt, Etienne Berthier, Fanny Brun, Wei-An Chao, Daniel Farinotti, Florent Gimbert, Wanqin Guo, Christian Huggel, Jeffrey S. Kargel, Gregory J. Leonard, Lide Tian, Désirée Treichler, and Tandong Yao. Massive collapse of two glaciers in western Tibet in 2016 after surge-like instability. *Nature Geoscience*, 11:114–120, 2018. doi: 10.1038/s41561-017-0039-7.

[4] Oldrich Hungr, Serge Leroueil, and Luciano Picarelli. The Varnes classification of landslide types, an update. *Landslides*, 11:167–194, 2014. doi: 10.1007/s10346-013-0436-y.

[5] M. J. Westoby, N. F. Glasser, J. Brasington, M. J. Hambrey, D. J. Quincey, and J. M. Reynolds. Modelling outburst floods from moraine-dammed glacial lakes. *Earth-Science Reviews*, 134:137–159, 2014. doi: 10.1016/j.earscirev.2014.03.009.

[6] Kristen L. Cook, Christoff Andermann, Florent Gimbert, Basanta Raj Adhikari, and Niels Hovius. Glacial lake outburst floods as drivers of fluvial erosion in the Himalaya. *Science*, 362(6410):53–57, 2018. doi: 10.1126/science.aat4981.

[7] Georg Veh, Oliver Korup, and Ariane Walz. Hazard from Himalayan glacier lake outburst floods. *Proceedings of the National Academy of Sciences*, 117(2):907–912, 2020. doi: 10.1073/pnas.1914898117.

[8] Martin Mergili, Michel Jaboyedoff, José Pullarello, and Shiva P. Pudasaini. Back calculation of the 2017 Piz Cengalo–Bondo landslide cascade with r.avaflow: what we can do and what we can learn. *Natural Hazards and Earth System Sciences*, 20:505–520, 2020. doi: 10.5194/nhess-20-505-2020.

[9] J. S. Kargel, G. J. Leonard, D. H. Shugar, U. K. Haritashya, A. Bevington, E. J. Fielding, K. Fujita, M. Geertsema, E. S. Miles, J. Steiner, E. Anderson, S. Bajracharya, G. W. Bawden, D. F. Breashears, A. Byers, B. Collins, M. R. Dhital, A. Donnellan, T. L. Evans, M. L. Geai, M. T. Glasscoe, D. Green, D. R. Gurung, R. Heijenk, A. Hilborn, K. Hudnut, C. Huyck, W. W. Immerzeel, Liming Jiang, R. Jibson, A. Kääb, N. R. Khanal, D. Kirschbaum, P. D. A. Kraaijenbrink, D. Lamsal, Shiyin Liu, Mingyang Lv, D. McKinney, N. K. Nahirnick, Zhuotong

Nan, S. Ojha, J. Olsenholler, T. H. Painter, M. Pleasants, K. C. Pratima, Q. I. Yuan, B. H. Raup, D. Regmi, D. R. Rounce, A. Sakai, Donghui Shangguan, J. M. Shea, A. B. Shrestha, A. Shukla, D. Stumm, M. van der Kooij, K. Voss, Xin Wang, B. Weihs, D. Wolfe, Lizong Wu, Xiaojun Yao, M. R. Yoder, and N. Young. Geomorphic and geologic controls of geohazards induced by Nepal's 2015 Gorkha earthquake. *Science*, 351(6269):aac8353, 2016. doi: 10.1126/science.aac8353.

[10] C. Huggel, S. Zgraggen-Oswald, W. Haeberli, A. Kääb, A. Polkvoj, I. Galushkin, and S. G. Evans. The 2002 rock/ice avalanche at kolka/karmadon, russian caucasus: assessment of extraordinary avalanche formation and mobility, and application of quickbird satellite imagery. *Natural Hazards and Earth System Sciences*, 5:173–187, 2005. doi: 10.5194/nhess-5-173-2005.

[11] Rosanna Sosio, Giovanni B. Crosta, and Oldrich Hungr. Complete dynamic modeling calibration for the thurwieser rock avalanche (italian central alps). *Engineering Geology*, 100:11–26, 2008. doi: 10.1016/j.enggeo.2008.02.012.

[12] Demian Schneider, Roland Kaitna, William E. Dietrich, Leslie Hsu, Christian Huggel, and Brian W. McArdell. Frictional behavior of granular gravel–ice mixtures in vertically rotating drum experiments and implications for rock–ice avalanches. *Cold Regions Science and Technology*, 69:70–90, 2011. doi: 10.1016/j.coldregions.2011.07.001.

[13] Shiva P. Pudasaini and Michael Krautblatter. A two-phase mechanical model for rock–ice avalanches. *Journal of Geophysical Research: Earth Surface*, 119:2272–2290, 2014. doi: 10.1002/2014JF003183.

[14] Geo-PERA. Bhote koshi flood 2026: a reconstruction from open satellite data. `https://geopera.com/blog/bhote-koshi-flood-2026-satellite-analysis`, 2026. Accessed September 2026.

[15] EarthScope Consortium. Rapid landslide force inversion for the 26 august 2026 langtang event, 2026. Web product, accessed September 2026.

[16] Göran Ekström and Colin P. Stark. Simple scaling of catastrophic landslide dynamics. *Science*, 339:1416–1419, 2013. doi: 10.1126/science.1232887.

[17] Kate Allstadt. Extracting source characteristics and dynamics of the August 2010 Mount Meager landslide from broadband seismograms. *Journal of Geophysical Research: Earth Surface*, 118:1472–1490, 2013. doi: 10.1002/jgrf.20110.

[18] S. G. Evans, O. V. Tutubalina, V. N. Drobyshev, S. S. Chernomorets, S. McDougall, D. A. Petrakov, and O. Hungr. Catastrophic detachment and high-velocity long-runout flow of kolka glacier, caucasus mountains, russia in 2002. *Geomorphology*, 105:314–321, 2009. doi: 10.1016/j.geomorph.2008.10.008.

[19] Pranay Lal. Himalayan ice-rock avalanche: how a 2026 langtang bedrock collapse turned into a deadly debris flow. `https://www.downtoearth.org.in/natural-disasters/when-rock-flows-like-a-river`, 2026. Down To Earth, accessed September 2026.

[20] European Space Agency. Copernicus dem glo-30, 2021.

[21] R. Barnes, C. Lehman, and D. Mulla. Priority-flood: An optimal depression-filling and watershed-labeling algorithm for digital elevation models. *Computers & Geosciences*, 62:117–127, 2014.

[22] European Space Agency. Sentinel-2 msi level-2a imagery, august 2026, 2026.

[23] E. Audusse, F. Bouchut, M.-O. Bristeau, R. Klein, and B. Perthame. A fast and stable well-balanced scheme with hydrostatic reconstruction for shallow water flows. *SIAM Journal on Scientific Computing*, 25(6):2050–2065, 2004.

[24] Richard M. Iverson. The physics of debris flows. *Reviews of Geophysics*, 35(3):245–296, 1997. doi: 10.1029/97RG00426.

[25] Jim S. O'Brien and Pierre Y. Julien. Laboratory analysis of mudflow properties. *Journal of Hydraulic Engineering*, 114:877–887, 1988. doi: 10.1061/(ASCE)0733-9429(1988)114:8(877).

[26] Pierre Y. Julien and Yongqiang Lan. Rheology of hyperconcentrations. *Journal of Hydraulic Engineering*, 117:346–353, 1991. doi: 10.1061/(ASCE)0733-9429(1991)117:3(346).

[27] UNOSAT. Product 4260: Langtang rock-ice avalanche and flood, affected surface and detachment zone, nepal, 2026. United Nations Satellite Centre.

[28] NDRRMA. Rasuwa flood situation report 01, 2026. 1 September 2026.

[29] Sunim Acharya. The Bhote Koshi–Trishuli flash flood of 26 August 2026, Rasuwa, Nepal: data and analysis code. Zenodo, version 1.0.0, 29 August 2026, 2026.

[30] Q. Liu, A. Khatri, A. Lord, M. Ghouli, N. Thapa, J. Steiner, W. W. Immerzeel, and S. Allen. Rapid hazard assessment report NP3: ice–rock avalanche and flood, Lirung range, Bhote Koshi, Nepal–China border. Technical report, HiRISK, Asian Mountain Academic Alliance, 2026. Last update 28 August 2026.

[31] Donghua Xu. The 26 August 2026 Langtang Lirung ice–rock avalanche and its transboundary cascade: a multi-source observational reconstruction in the Bhote Koshi basin. EarthArXiv preprint, version 2, 1 September 2026, 2026.

Supplementary Information for: A rock–ice avalanche without yield strength caused the 2026 Bhote Koshi–Trishuli flood, Nepal

Hyoseok Park[1,*]
[1]Department of Physics, Chungnam National University, Daejeon, Republic of Korea
*phs137@o.cnu.ac.kr

Preprint, not peer reviewed. Submitted to EarthArXiv, September 2026.

Supplementary Notes

Supplementary Note 1: two-phase test

The two-phase model solves, on the same grid, the equations of Pitman and Le [1] in the form of Pudasaini [2]: solid and fluid phases with one free surface and density ratio $\gamma = \rho_f/\rho_s = 0.4$, the solid carrying the granular pressure $\frac{1}{2}(1-\gamma)g\alpha h^2$ (α, solid volume fraction) and the buoyancy share $\gamma\alpha$ of the total pressure force, the fluid the share $1-\alpha$, coupled by linear drag with terminal velocity U_T, with Coulomb resistance $\mu(1-\gamma)(1-p)gh_s$ on the solid where p is the excess pore-pressure ratio, prescribed at the release and dissipating on the timescale h^2/D [3]. With $p_0 = 1$ the solid is liquefied by assumption; the test asks whether, given that state, phase separation changes the flow. Supplementary Table S1 lists the runs; for h of tens of metres and $D = 10^{-3}$ m^2/s the dissipation time exceeds the event and the fourth run differs from the first by one output interval.

Supplementary Note 2: friction coupled to the water content

To test whether the bulk meltwater could have removed the friction, the basal friction was made to fall with the local water fraction $w = 1-c$, $\mu = \mu_{\mathrm{dry}}(1 - w/w_{\mathrm{sat}})_+$, on the 30 m grid with the production release and energy-conserving melting, for μ_{dry} of 0.1 and 0.2, w_{sat} of 0.2 and 0.36 (pore saturation of a packed mass) and ice fractions of 0.2 and 0.4. The arrivals of the four variants are in Supplementary Table S2.

Supplementary Note 3: flow height and speed in the gorge

In the tributary gorge above the Bhote Koshi confluence the trimlines mapped from 2 m imagery stand 48–70 m above the channel [4], and the reconstruction gives a median maximum flow height of 61 m over the first 22 km (median over 1 km bins of the maximum height on the thalweg). Between Rasuwagadhi and Syabrubesi the Planet 12 m disturbance mapping places the trimline a median 27 m above the channel (23 one-kilometre bins), and super-elevation at 13 bends mapped from 2 m imagery between 12 and 39 km from the source gives flow speeds of 30–53 m/s. The reconstruction gives a maximum flow height of 1.26 times the trimline (Pearson correlation 0.34 between the 23 bin pairs) and a maximum depth-averaged speed of 0.67 times the super-elevation value (Supplementary Fig. S4); super-elevation records the surface velocity at the outer bank, which exceeds the depth-averaged speed by a factor of this order [5]. Both ratios say that the modelled section is wider and slower than the real gorge, which is what the 30 m radar terrain resolves and what the low calibrated roughness compensates. The released 2 m elevation-change product of the channel between 20 and 46 km from the source shows $3.1 \times 10^6\,\mathrm{m}^3$ of erosion against $0.8 \times 10^6\,\mathrm{m}^3$ of deposition; the reconstruction gives $5.5 \times 10^6\,\mathrm{m}^3$ and $2.0 \times 10^6\,\mathrm{m}^3$ in the same reach. The material did not stop in the gorge.

Supplementary Note 4: volume ledger

Release 35.4×10^6 m^3 (28.3×10^6 m^3 rock, 7.1×10^6 m^3 ice); river inflow over 8 h 73×10^6 m^3; entrained channel fill 30×10^6 m^3, of which 5.5×10^6 m^3 in the 20–46 km reach mapped by GeoPERA; melted ice 7.0×10^6 m^3 (no volume change); settled solids 20×10^6 m^3, all below Betrawati, at a thickness of 1–2 m over the valley floor between Betrawati and Galchhi with local piles of 5–20 m, against a mapped deposition of 0.8×10^6 m^3 and typical thickness of 0.4–4 m in the Syabrubesi reach. Mixture passing the transects over 8 h above the base flow: Rasuwagadhi 38×10^6 m^3, Syabrubesi 50×10^6 m^3, Betrawati 43×10^6 m^3, Galchhi 46×10^6 m^3 (corridor model) and Devghat 16–22 $\times 10^6$ m^3 (routed ensemble); the difference between Galchhi and Devghat is the valley-floor storage of the routing.

Supplementary Tables

Table S1: Two-phase test on the 30 m grid: first arrival (s, output every 60 s).

run	U_T (m/s)	p_0	Gyirong	Rasuwagadhi	Syabrubesi
phases locked	1	1	360	360	900
phases free	20	1	360	360	900
partly drained	1	0.85	480	540	2400
dissipating, $D = 10^{-3}$ m^2/s	1	1	360	420	960
observed window			373–553	170–770	770–1370

Table S2: Friction coupled to the water content: first arrival (s) on the 30 m grid with the production release, energy-conserving melting and a friction $\mu = \mu_{\text{dry}}(1 - w/w_{\text{sat}})_+$. Observed windows: Gyirong 373–553 s, Rasuwagadhi 170–770 s, Syabrubesi 770–1370 s.

run	μ_{dry}	w_{sat}	ice fraction	Gyirong	Rasuwagadhi	Syabrubesi
a	0.2	0.36	0.2	1680	1860	never
b	0.2	0.20	0.2	540	600	2100
c	0.1	0.36	0.2	720	840	2880
d	0.2	0.36	0.4	1320	1500	3600

Supplementary Figures

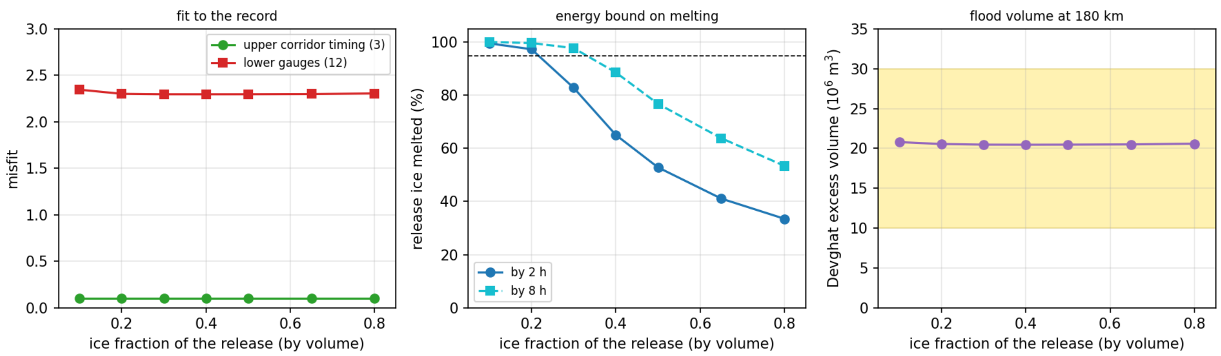

Figure S1: What the record says about the ice fraction. For releases of 10–80% ice by volume without yield strength and with the full heat budget: misfit of the upper-corridor arrivals and of the lower-gauge criteria (left), fraction of the release ice melted within two hours and within eight hours (centre, dashed line at 95%) and the excess volume at Devghat (right, band: observed 10–30 $\times 10^6$ m^3). The gauges do not resolve the ice fraction; the energy bound on melting does.

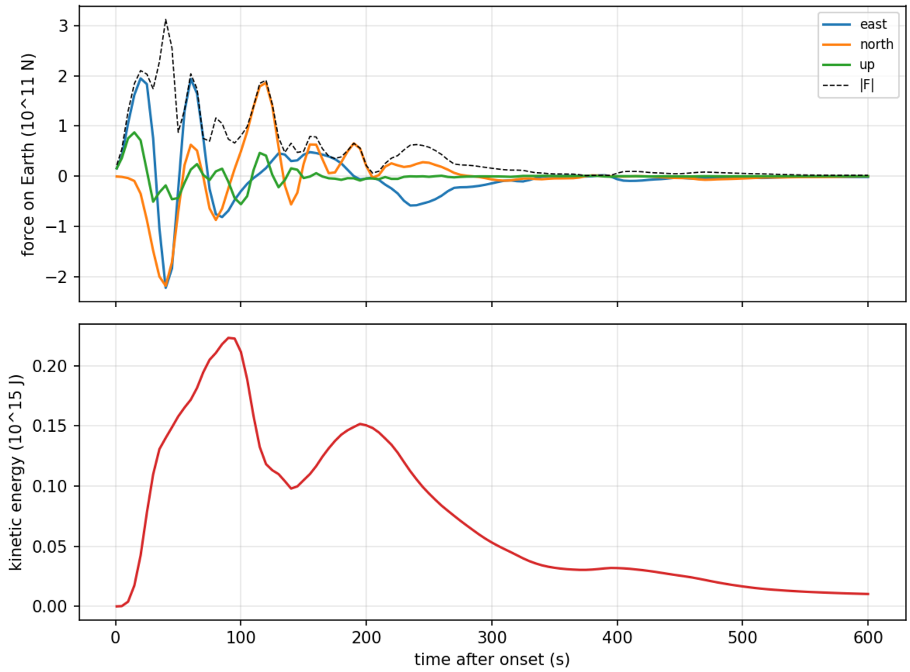

Figure S2: Force on the Earth and kinetic energy of the flow. Components and magnitude of $-\mathrm{d}\mathbf{P}/\mathrm{d}t$ during the first 600 s from the 30 m run stored every 5 s, and the kinetic energy of the moving mass. This run releases the mass at rest; the peak of 3.1×10^{11} N at 40 s is the impact on the valley floor (3.3×10^{11} N at 35 s when the mass is released with the free-fall speed, as in the inversion runs), and the first 30 s are the prescribed release.

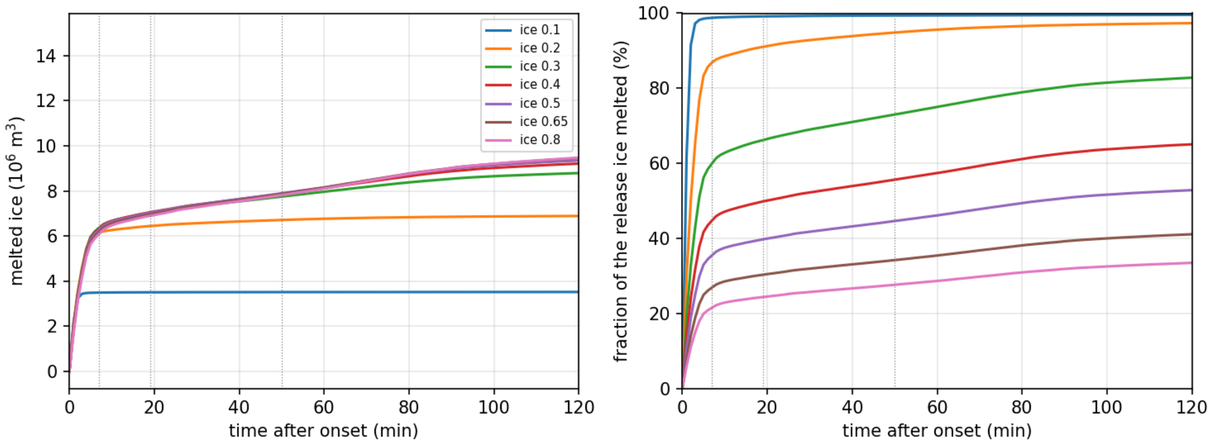

Figure S3: Melting of the release ice. Melted volume (left) and fraction of the release ice melted (right) for releases of 10–80% ice by volume on the corridor grid with the whole mechanical-energy loss delivered to the mixture as heat, and, dashed, the 30 m run with 25% ice; dotted, the same 30 m run with only the bed-friction work as heat. Vertical lines: Gyirong Port, Syabrubesi, Betrawati.

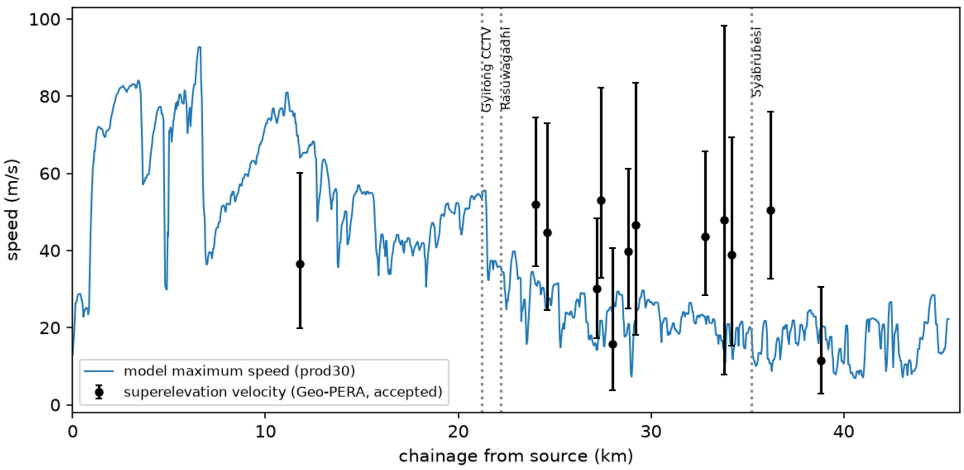

Figure S4: Speed along the gorge. Maximum modelled depth-averaged speed along the corridor (30 m run) against the super-elevation velocities at 13 bends with their reported ranges.

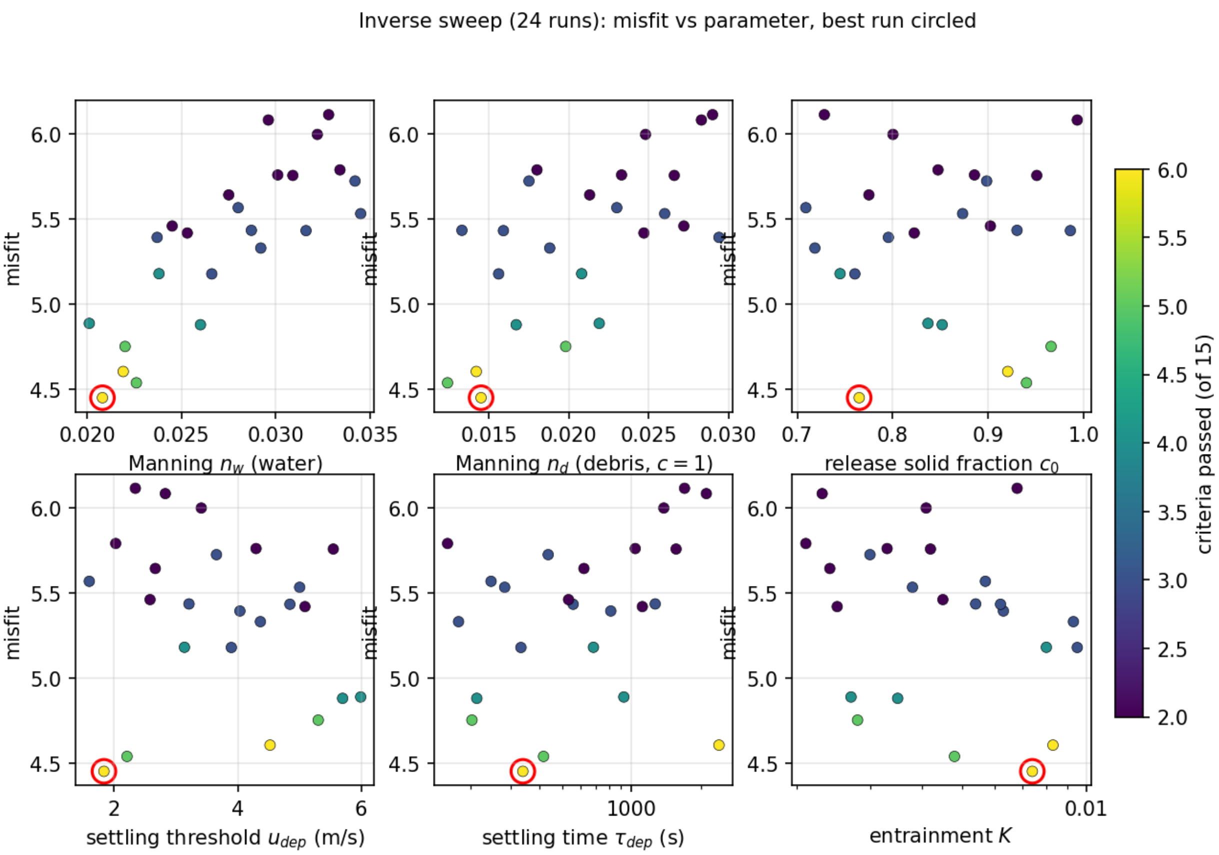

Figure S5: Corridor parameter sweep. Misfit of 24 corridor runs against all criteria as a function of each parameter (Latin-hypercube sample; colour, number of criteria met; circle, best run). The water roughness controls the misfit and is driven to the sampled lower bound: the 60 m grid alone cannot convey the wave fast enough.

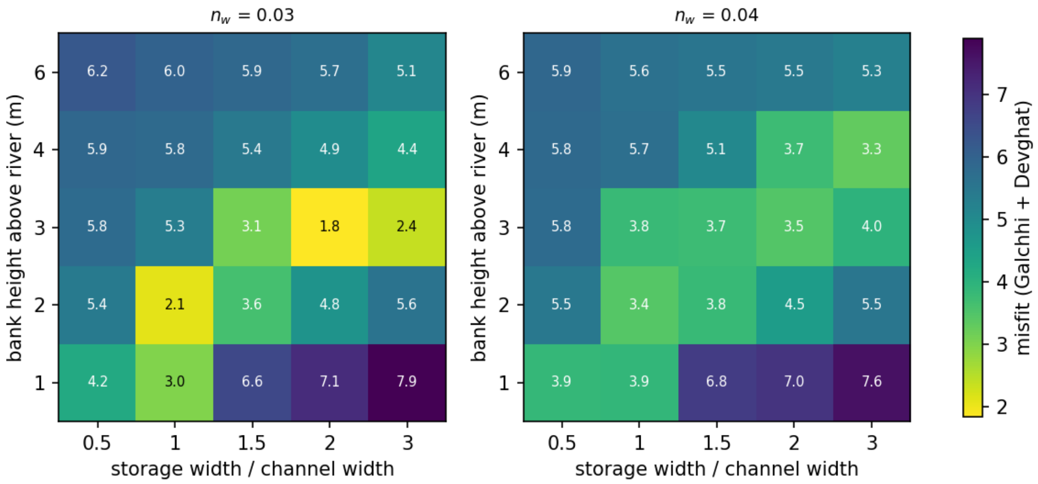

Figure S6: Storage parameters fitted on Galchhi and Devghat alone. Misfit of the routed surge against the eight Galchhi and Devghat criteria over the 5×5 grid of bank height and storage width, for two channel roughnesses; the low-misfit band follows constant storage capacity.

References

[1] E. Bruce Pitman and Long Le. A two-fluid model for avalanche and debris flows. *Philosophical Transactions of the Royal Society A*, 363:1573–1601, 2005. doi: 10.1098/rsta.2005.1596.

[2] Shiva P. Pudasaini. A general two-phase debris flow model. *Journal of Geophysical Research: Earth Surface*, 117:F03010, 2012. doi: 10.1029/2011JF002186.

[3] Richard M. Iverson and David L. George. A depth-averaged debris-flow model that includes the effects of evolving dilatancy. i. physical basis. *Proceedings of the Royal Society A*, 470: 20130819, 2014. doi: 10.1098/rspa.2013.0819.

[4] Geo-PERA. Bhote koshi flood 2026: a reconstruction from open satellite data. `https://geopera.com/blog/bhote-koshi-flood-2026-satellite-analysis`, 2026. Accessed September 2026.

[5] Adam B. Prochaska, Paul M. Santi, Jerry D. Higgins, and Susan H. Cannon. A study of methods to estimate debris flow velocity. *Landslides*, 5:431–444, 2008. doi: 10.1007/s10346-008-0137-0.